



Simulated assessment of light transport through ischaemic skin flaps

Mark Main^a, Richard J.J. Pilkington^b, Graham M Gibson^c, Akhil Kallepalli^{c,*}

^a James Watt School of Engineering, University of Glasgow, Glasgow G12 8QQ, United Kingdom

^b Oral and Maxillofacial Surgery, Cumberland Infirmary, Carlisle CA2 7HY, United Kingdom

^c School of Physics and Astronomy, University of Glasgow, Glasgow G12 8QQ, United Kingdom

Received 15 February 2022; revised 25 February 2022; accepted in revised form 15 March 2022

Abstract

Currently, free flaps and pedicled flaps are assessed for reperfusion in postoperative care using colour, capillary refill, temperature, texture, and Doppler signal (if available). While these techniques are effective, they are prone to error due to their qualitative nature. In this research, different wavelengths of light were used to quantify the response of ischaemic tissue. The assessment provides indicators that are key to developing a point-of-care diagnostic device that is capable of observing reduced perfusion quantitatively. Detailed optical models of the layers of the skin were set up and appropriate optical properties assigned, with due consideration of melanin and haemoglobin concentration. A total of 24 models of healthy, perfused and perfusion-deprived tissue were used to assess the responses when illuminated with visible and near-infrared wavelengths of light. In addition to detailed fluence maps of photon propagation, a simple mathematical model is proposed to assess the differential propagation of photons in tissue; the optical reperfusion factor (ORF). The results show clear advantages of using light at longer wavelengths (red, near-infrared) and the inferences drawn from the simulations hold significant clinical relevance. The simulated scenarios and results consolidate the belief in a multi-wavelength, point-of-care diagnostic device, and inform its design to quantify blood flow in transplanted tissue. The modelling approach is applicable beyond the current research and can be used to investigate other medical conditions in the skin that can be mathematically represented. Through these, additional inferences and approaches to other point-of-care devices can be realised.

© 2022 The Authors. Published by Elsevier Ltd on behalf of The British Association of Oral and Maxillofacial Surgeons. This is an open access article under the CC BY license (<http://creativecommons.org/licenses/by/4.0/>).

Keywords: Maxillofacial; Optical diagnostics; Monte Carlo simulations; Postoperative care; Optical reperfusion factor

Introduction

Free tissue transfer has become the method of choice for the reconstruction of defects produced by the ablative treatment of cancer and, less commonly, trauma to the head and neck. It is a reliable method of reconstruction that results in improved postoperative function and aesthetic appearance.¹ The ideal flap monitoring system should be harmless to the patient and the flap. It should also be of low cost, and be rapidly responsive, accurate, reliable, and applicable to all types of flaps. The monitor should be equipped with a simple

display that would allow even the least experienced member of the team to easily recognise circulatory impairment. Attempts to develop such a device have been made in the past, but there remains a necessity to achieve all the above requirements in one system.^{2–6}

Many techniques for the postoperative monitoring of free-tissue transfers, both invasive and non-invasive, have been developed and evaluated in clinical settings, and in experimental free-flap models. Unfortunately, the level of evidence for their efficacy in clinical practice is often very low, and cost/benefit analyses are rare. The only accepted practice in this field seems to be the almost universal use of clinical bedside monitoring of free tissue transfer. This is supported by an overwhelming impression from the literature reviewed that clinical monitoring is the most practical and possibly the most reliable method.⁷

* Corresponding author.

E-mail addresses: Mark.Main@glasgow.ac.uk (M. Main), r.pilkington@nhs.net (R.J.J. Pilkington), Graham.Gibson@glasgow.ac.uk (G.M Gibson), Akhil.Kallepalli@glasgow.ac.uk (A. Kallepalli).

<https://doi.org/10.1016/j.bjoms.2022.03.004>

0266-4356/© 2022 The Authors. Published by Elsevier Ltd on behalf of The British Association of Oral and Maxillofacial Surgeons. This is an open access article under the CC BY license (<http://creativecommons.org/licenses/by/4.0/>).

In this article, Monte Carlo simulations were used to assess the interaction of visible and near-infrared wavelengths with healthy and ischaemic skin tissue, and to present the clinical relevance of optical technologies for free flap monitoring. The results of these simulations will assist in the future development of design strategies for a non-contact and safe point-of-care diagnostic device.

Methods

When light interacts with biological tissue, a combination of reflection, refraction, scattering, and absorption occurs (Fig. 1). To safely assess optical methods for diagnostics prior to clinical trials, Monte Carlo (MC) simulations have been widely used to simulate the interactions between light and tissue. In this assessment, a seven-layer tissue model (Fig. 1) representing the epidermis, dermis, and subcutaneous fat layers was built.⁸ To account for varying skin types, the melanin concentration was quantified by categorising the epidermis into three types, combining consecutive classifications on the Fitzpatrick scale.⁹ The dermis layer was modelled in two scenarios of healthy and ischaemic tissues, as was the case for failing skin flaps.¹⁰ The common optical properties are detailed in Table S1 (online only).

The optical properties of skin layers in the literature were critically analysed and chosen from multiple studies.¹¹⁻¹⁷ The absorption coefficient of the base layer (without absorbers), μ_a^{skin} (Equation (1)) depends on the wavelength of the incident light.¹¹ Subsequently, the contribution of melanin is accounted for through Equation (2). Combined,

Equation (3) gives the absorption coefficient of the epidermis layer. This was calculated for three scenarios of melanin volume fractions ($f_{melanin} = 0.037, 0.134, 0.305$). The absorption coefficient of the stratum corneum was calculated using Equation (4), which accounts for absorption due to water, baseline skin, and wavelength. Further, adopted from previous studies, the scattering properties of the epidermal layers were assigned to the models (Tables S2^{8,11} and S3^{8,11,17-19} online only). The concentration of water was denoted by C_{H_2O} .

$$\mu_a^{skin} = 7.84 \times 10^7 \times \lambda^{-3.255} [\lambda : nm] \tag{1}$$

$$\mu_a^{melanin} = 6.6 \times 10^{10} \times \lambda^{-3.3} [\lambda : nm] \tag{2}$$

$$\mu_a^{epidermis} = f_{melanin} \mu_a^{melanin} + (1 - f_{melanin}) \mu_a^{skin} \tag{3}$$

$$\mu_a^{stratum\ corneum} = ((0.1 - 0.3 \times 10^{-4} \lambda) + 0.125 \mu_a^{skin})(1 - C_{H_2O}) + C_{H_2O} \mu_a^{H_2O} \tag{4}$$

Mathematically, the absorption coefficient of the dermis layer is calculated as a total of its constituents. This includes the absorption due to water $\mu_a^{H_2O}$, oxygenated $\mu_a^{HbO_2}$ and deoxygenated μ_a^{Hb} blood, volume fraction of haemoglobin (γ) and blood oxygen saturation (S). The absorption coefficient for the dermis layer, $\mu_a^{dermis}(\lambda)$ is defined as:

$$\mu_a^{dermis}(\lambda) = (1 - S) \gamma C_{blood} \mu_a^{Hb}(\lambda) + S \gamma C_{blood} \mu_a^{HbO_2}(\lambda) + (1 - \gamma C_{blood}) C_{H_2O} \mu_a^{H_2O}(\lambda) + (1 - \gamma C_{blood})(1 - C_{H_2O}) \mu_a^0(\lambda) \tag{5}$$

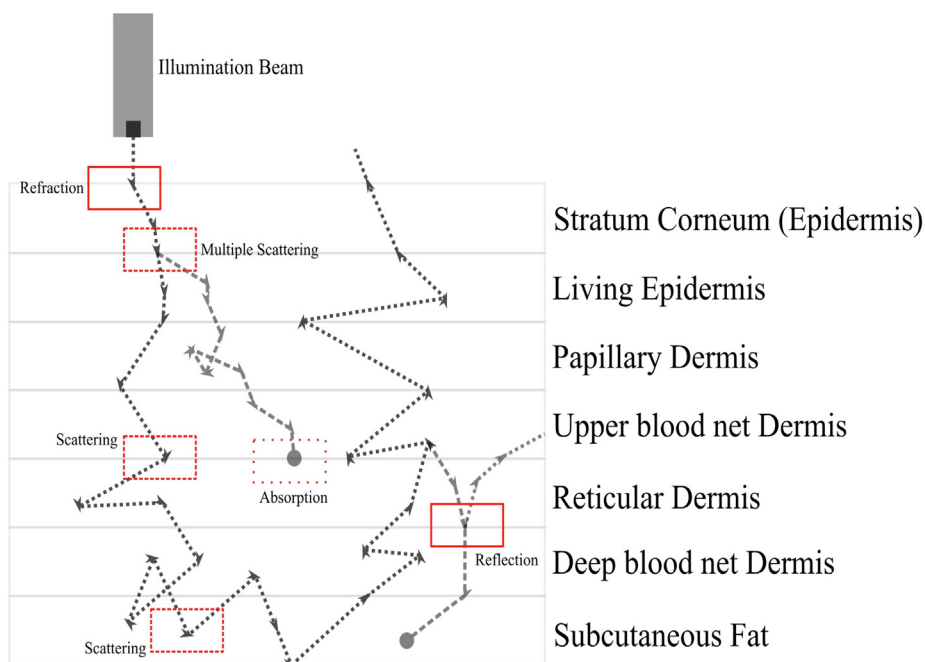


Fig. 1. Light encounters multiple interactions when propagating through biological tissue. These include absorption, scattering, and reflection at or within individual layers. This illustration shows an example of photon propagating through a multi-layer skin model. Each layer in the model is described by physical thickness (d), and optical properties, such as refractive index (η), absorption coefficient (μ_a), scattering coefficient (μ_s), and anisotropy (g). The model is adopted from Meglinski and Matcher (2002).⁸

The volume fractions of blood and water, C_{blood} and C_{H_2O} , were adopted from Meglinski and Matcher.⁸ The constituents of blood were quantified using γ , a factor determined by haematocrit (Ht), volume fraction of the red blood count (F_{RBC}) and the volume fraction of haemoglobin in individual red blood cells (F_{Hb}). This was defined as $\gamma = Ht \times F_{RBC} \times F_{Hb}$. The value for γ was kept consistent throughout all layer calculations with $Ht = 0.45$, $F_{RBC} = 0.99$, and $F_{Hb} = 0.25$, as this represented typical values found in healthy tissue.

A failing skin flap primarily experiences a reduction in blood flow. To model this, C_{blood} values for layers were reduced by half to 0.02, 0.15, 0.02, and 0.05. Using Equation (5), the optical properties of an ischaemic flap were calculated (Tables S4 and S5 online only). Finally, the optical properties assigned to the subcutaneous fat layer were directly adopted from the literature.⁸

The seven-layer tissue models considered three scenarios of melanin distribution and two scenarios of blood flow. Each model was assessed by illumination with a billion photons at four distinct wavelengths of 480 nm (blue), 520 nm (green), 650 nm (red) and 950 nm (near-infrared). Combined, our study has presented a detailed assessment of photon propagation in a total of 24 models. Each model and the corresponding results are accessible online.²⁰

$$ORF_{1-2} = \frac{|\lambda_1 - \lambda_2|}{\lambda_1 + \lambda_2} \quad (6)$$

After the simulations were complete, a new mathematical factor was defined to analyse the results. The optical reperfusion factor (ORF, Equation (6)) was used to quantify the differential interactions of light with healthy and ischaemic tissue (Fig. 2). The experimental analogy of clinical relevance here is that every flap site and optical system's field of view will include the flap itself and the surrounding healthy tissue. The corresponding measurements at multiple wavelengths from different sites are possible for clinical use.

Results and Discussion

By comparing each of the four wavelengths used in the simulations, substantial variation could be seen in tissue absorption and depth penetration (Fig. S1 online only). For wavelengths 480 nm and 520 nm, there was a high degree of absorption at beam incidence, which resulted in a lower degree of penetration to deeper layers. A few photons did propagate but these did not hold any significance in a clinical or experimental context. This was due to the high energy deposition in the upper layers, which could cause photochemical and photobiological damage under conditions of prolonged exposure, or when using high-power light sources.

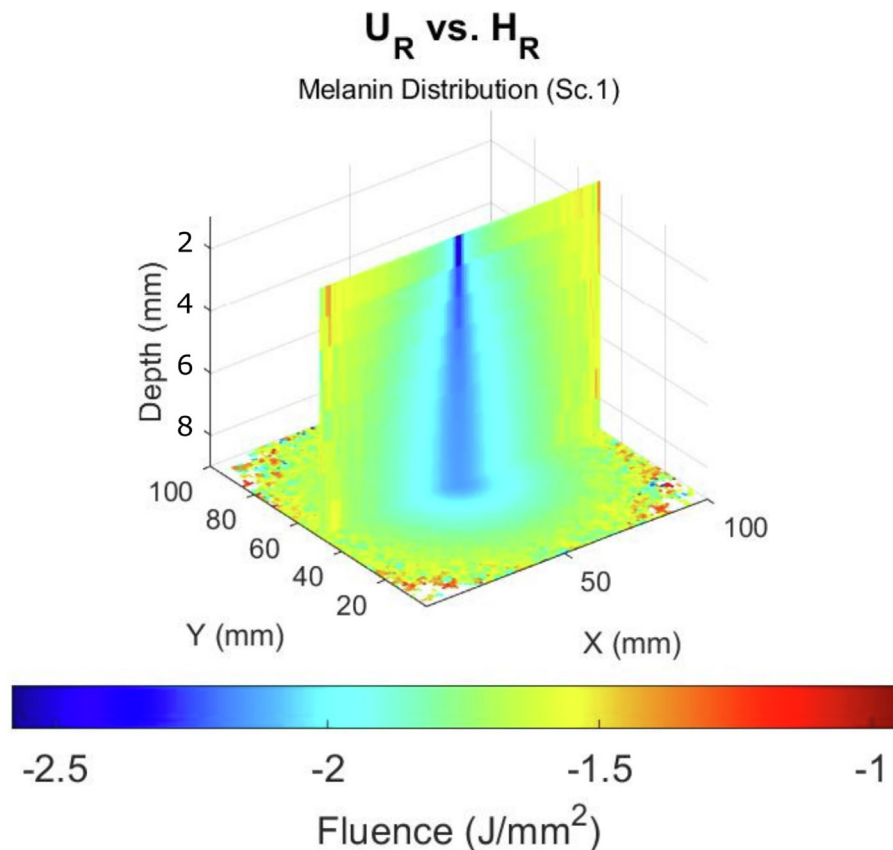


Fig. 2. The optical reperfusion factor is calculated for red wavelength illumination of healthy and ischaemic tissue. Equation (6) was used to create the comparison and show the variation between the results. Healthy dermal perfusion is denoted with H, while ischaemic tissue models are denoted with U.

When considering longer wavelengths such as red and near-infrared, photons propagate deeper into the tissue. Therefore, the dermis layer with varied blood perfusion characteristics can be investigated. The lateral absorption when using red light is reduced when compared with blue and green wavelengths. With sufficient penetration and low lateral absorption in both healthy and unhealthy tissue, this suggests that red light at 650 nm would be a suitable wavelength to use when imaging a patch of tissue without causing any damage at skin-safe powers. Similarly, near-infrared light has both high penetration and lower lateral absorption, indicating it could be useful for imaging tissue patches (Fig. S1 online only).

Individually, each of the wavelengths provides inferences regarding photon propagation in different conditions of melanin distribution and/or blood perfusion. However, in a clinical context, a single wavelength system cannot achieve a quantitative differentiation of healthy and ischaemic tissue because variations of absorption from the skin site can occur for many reasons other than blood flow changes alone. Therefore, to quantitatively assess the variation of blood flow in the flap, multiple wavelengths and/or different measurements must be taken. The measurements taken will be assessed by the proposed optical reperfusion factor (ORF), given in Equation (6). The normalising factor considers various combinations of measurements at different wavelengths.

When the ORF maps are compared (Fig. S2 online only), substantial variation can be seen further away from the point of incidence (a–f). The variations imply a high degree of absorption when considering these combinations relatively, and therefore result in greater differences. For instance, deeper penetration of near-infrared wavelength compared with surface absorption of green photons results in a higher difference deeper in the tissue model. The variation in absorption between red and near-infrared is less significant at incidence, as indicated by a small region of low fluence.

Key differences can be seen in Fig. S2 (g and h). These compare combinations of healthy and ischaemic tissue models in near-infrared and red wavelengths. Promisingly, notable differences are evident in both cases. In Fig. S2 (g) (online only), the variation in energy deposition is not significant beyond where the beam enters the tissue model, that is, at the site of incidence. In Fig. S2 (h) (online only) comparing healthy and ischaemic conditions under red light illumination, there is far greater variation in energy deposition. Two distinct regions within this model demonstrate the high absorption rate of red light by haemoglobin. The central column has little variation in energy deposition, which is expected due to the smaller distance travelled, reducing the absorption and scattering of the light. Further, melanin does not absorb red light as much as blue and green so deep penetration is seen in red wavelengths and beyond. The area to note is the region of higher difference surrounding this central column. As the distance increases from the entry point of the incident beam, the variation in energy deposition increases. This demonstrates the results of a difference in

blood perfusion within tissue, as the variance in absorption increases as a function of distance from the entry point of the incident beam.

To highlight the result of significance, the case of observing healthy and ischaemic blood perfusion under red illumination is highlighted (Fig. S2 online only). A linear increase of variance is observed in the ORF map. A combination of red and near-infrared wavelength illumination and measurement of absorption within healthy and ischaemic tissue is the key ‘take-away’ from the simulated Monte Carlo assessments.

Conclusions

The purpose of this research was to investigate whether optical methods can be used to determine varying blood volumes within a section of skin tissue. By varying the optical properties of tissue and taking account of a reduction in blood volume, Monte Carlo simulations were used to analyse a seven-layer tissue model. The results of these simulations²⁰ detail both the interaction of light in this tissue as well as comparisons made between varying wavelengths and blood perfusion. Analysis of the data shows that across wavelengths, and with single wavelengths, a variation can be found between healthy and ischaemic tissue. The variation found using the optical reperfusion factor is sufficient to allow an experimental study to be conducted.

The inferences from this study lay the foundations for future analyses that will include the blood vessels in the tissue models, and serve as input to develop a multi-wavelength system using red and near-infrared light to monitor reperfusion. This can be done by collecting measurements from within and beyond the flap boundaries. The measurements collected from the surrounding tissue will act as a healthy reference to a potentially ischaemic free flap. This will result in a quantitative analysis of blood perfusion within the transplanted tissue using a non-contact and safe point-of-care diagnostic device.

Acknowledgements

We wish to acknowledge the support from the Research Fund awarded by the Endowments Sub Committee of the British Association of Oral and Maxillofacial Surgeons (2021), EPSRC Research Council funding [EP/T517896/1, EP/M01326X/1], and the Royal Society. We would also like to thank Dr Qianqian Fang, Shijie Yan, and Dr Yaoshen Yuan (Computational Optics and Translational Imaging Lab, College of Engineering, Northeastern University, Boston) for their invaluable advice and assistance with MCX, the Monte Carlo simulation platform used in this research.

Data availability

The MATLAB codes for each model and the full set of results are available online.²⁰

Conflict of interest

We have no conflicts of interest.

Ethics statement/confirmation of patients permission

Not applicable.

Appendix A. Supplementary data

Supplementary data to this article can be found online at <https://doi.org/10.1016/j.bjoms.2022.03.004>.

References

1. Devine JC, Potter LA, Magennis P, et al. Flap monitoring after head and neck reconstruction: evaluating an observation protocol. *J Wound Care* 2001;**10**:525–529.
2. Holmer A, Tetschke F, Marotz J, et al. Oxygenation and perfusion monitoring with a hyperspectral camera system for chemical based tissue analysis of skin and organs. *Physiol Meas* 2016;**37**:2064–2078.
3. Fox PM, Zeidler K, Carey J, et al. White light spectroscopy for free flap monitoring. *Microsurgery* 2013;**33**:198–202.
4. Whitaker IS, Pratt GF, Rozen WH, et al. Near infrared spectroscopy for monitoring flap viability following breast reconstruction. *J Reconstr Microsurg* 2012;**28**:149–154.
5. Repež A, Oroszy D, Arnež ZM. Continuous postoperative monitoring of cutaneous free flaps using near infrared spectroscopy. *J Plast Reconstr Aesthet Surg* 2008;**61**:71–77.
6. Calin MA, Bioangiu IC, Parasca SV, et al. Blood oxygenation monitoring using hyperspectral imaging after flap surgery. *Spectroscopy Letters* 2017;**50**:150–155.
7. Abdel-Galil MD. Postoperative monitoring of microsurgical free-tissue transfers for head and neck reconstruction: a systematic review of current techniques — part II. Invasive techniques. *Br J Oral Maxillofac Surg* 2009;**47**:438–442.
8. Meglinski IV, Matcher SJ. Quantitative assessment of skin layers absorption and skin reflectance spectra simulation in the visible and near-infrared spectral regions. *Physiol Meas* 2002;**23**:741–753.
9. Kallepalli A, Halls J, James DB, et al. An ultrasonography-based approach for tissue modelling to inform photo-therapy treatment strategies. *J Biophotonics* 2022;**15**:e202100275.
10. Mignon C, Tobin DJ, Zeitouny M, et al. Shedding light on the variability of optical skin properties: finding a path towards more accurate prediction of light propagation in human cutaneous compartments. *Biomed Opt Express* 2018;**9**:852–872.
11. Jacques SL. Optical properties of biological tissues: a review. *Phys Med Biol* 2013;**58**:R37–R61.
12. Svaasand LO, Norvang LT, Fiskerstrand EJ, et al. Tissue parameters determining the visual appearance of normal skin and port-wine stains. *Lasers Med Sci* 1995;**10**:55–65.
13. Salomatina E, Jiang B, Novak J, et al. Optical properties of normal and cancerous human skin in the visible and near-infrared spectral range. *J Biomed Opt* 2006;**11**:064026.
14. Anderson RR, Parrish JA. The optics of human skin. *J Invest Dermatol* 1981;**77**:13–19.
15. Bashkatov AN, Genina EA, Kochubey VI, et al. Optical properties of human skin, subcutaneous and mucous tissues in the wavelength range from 400 to 2000 nm. *J Phys D: Appl Phys* 2005;**38**:2543–2555.
16. Ding H, Lu JQ, Wooden WA, et al. Refractive indices of human skin tissues at eight wavelengths and estimated dispersion relations between 300 and 1600 nm. *Phys Med Biol* 2006;**51**:1479–1489.
17. Simpson CR, Kohl M, Essenpreis M, et al. Near-infrared optical properties of ex vivo human skin and subcutaneous tissues measured using the Monte Carlo inversion technique. *Phys Med Biol* 1998;**43**:2465–2478.
18. Altshuler G, Smirnov M, Yaroslavsky I. Lattice of optical islets: a novel treatment modality in photomedicine. *J Phys D: Appl Phys* 2005;**38**:2732–2747.
19. Karsten AE, Smit JE. Modeling and verification of melanin concentration on human skin type. *Photochem Photobiol* 2012;**88**:469–474.
20. Main M, Pilkington RJ, Gibson GM, et al. Simulated assessment of light transport through ischaemic skin flaps (dataset). University of Glasgow 2022. DOI: 10.5525/gla.researchdata.1247.